

# A Mobile Quad-Arm Robot ARMS: Wheel-Legged Tripedal Mobility and Quad-Arm Manipulation

Hisayoshi Muramatsu, Keigo Kitagawa, Jun Watanabe, and Ryohei Hisashiki

**Abstract**—This letter proposes a mobile quad-arm robot: ARMS that unifies wheel-legged tripedal mobility, wheeled mobility, and quad-arm manipulation. The four arms have different mechanics and are designed to be general-purpose arms to enable the wheel-legged hybrid mobilities and manipulation. The three-degree-of-freedom (DOF) front arm has an active wheel, which is used for wheel-legged tripedal walking and wheel driving with passive wheels attached to the torso. The three-DOF rear arms are series elastic arms, which are used for wheel-legged tripedal walking, object grasping, and manipulation. The two-DOF upper arm is used for manipulation only; its position and orientation are determined by coordinating all arms. Each motor is controlled by an angle controller and trajectory modification with angle, angular velocity, angular acceleration, and torque constraints. ARMS was experimentally validated on the basis of the following four tasks: wheel-legged walking, wheel-driving, wheel-driving with grasping, and carrying a bag.

**Index Terms**—Hybrid mobility, wheel-legged robots, legged robots, wheeled robots, mobile manipulation, mechanical design, motion control

## I. INTRODUCTION

Robots are expected to acquire general mobility and general task capability to perform various tasks across various environments. Despite the demand, most existing robots are typically task-oriented, such as legged robots for rough terrain [1]–[5], wheeled robots for flat terrain [6], [7], and humanoid robots for manipulation tasks [8]–[10]. To enhance the versatility of a robot, mobile manipulation robots with hybrid mobility and manipulation capability have been developed.

For the unification of the legged mobility and manipulation, quadrupedal robots, such as RoboSimian [11] and ALPHRED [12], have four general-purpose limbs. They can perform both quadrupedal walking and manipulation, such as grasping and valve turning without additional limbs, which is effective in reducing the weight of the robots.

Moreover, for the unification of the legged mobility and wheeled mobility, quadrupedal robots, such as RoboSimian [11], CENTAURO [13], ANYmal [14], [15], BITNAZA II [16], and a wheel-legged robot [17], have hybrid mobility that combines legged and wheeled mobilities. RoboSimian [11] has two active wheels on its body and two passive wheels on its limbs, and the other robots have active wheels attached to the tips of their legs. Additionally,

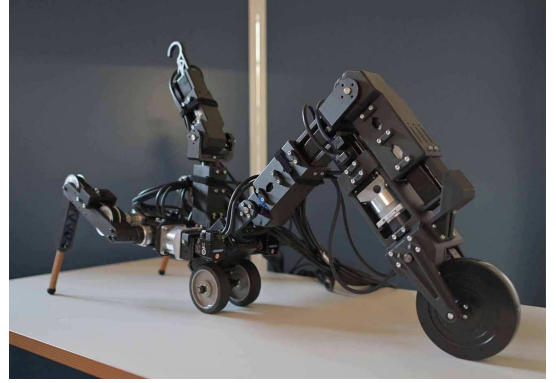


Fig. 1. Mobile quad-arm robot: ARMS.

there are wheel-legged bipedal robots [18]–[21], wheel-legged hexapedal robot [22], and wheeled robots that can transform their wheels to legs [23]–[26] for the hybrid mobility.

In previous robots, the unification of hybrid mobility and manipulation effectively enhanced the versatility, but previous legged types were unstable bipedal types or redundant quadrupedal and hexapedal types. Moreover, the unification of the legged mobility, wheeled mobility, and manipulation capability is rare and is realized only by quadrupedal robots, such as RoboSimian [11]. Therefore, robots unifying tripedal hybrid mobility, wheeled mobility, and manipulation capability have not been developed yet.

This letter proposes a mobile quad-arm robot: ARMS, which unifies wheel-legged tripedal mobility, wheeled mobility, and quad-arm manipulation. The four arms have different mechanics and are designed to be general-purpose arms for hybrid mobility and manipulation. The three-degrees-of-freedom (DOF) front arm has an active wheel, which is used for the wheel-legged tripedal walking and wheel driving with passive wheels attached to the torso. The three-DOF rear arms are series elastic arms, which are used for the wheel-legged tripedal walking, object grasping, and manipulation. The two-DOF upper arm is used for manipulation only; its position and orientation are determined by coordinating all arms. ARMS has 12 motors for the four arms and active wheel, and each motor is controlled by an angle controller and trajectory modification with angle, angular velocity, angular acceleration, and torque constraints.

Compared to the aforementioned robots, ARMS achieves the unification of the wheel-legged tripedal mobility, wheeled

This work was supported by JKA Japan. (Corresponding author: Hisayoshi Muramatsu). H. Muramatsu, K. Kitagawa, J. Watanabe, and R. Hisashiki are with Mechanical Engineering Program, Hiroshima University, Higashihiroshima 739-8527, Japan (e-mail: muramatsu@hiroshima-u.ac.jp).

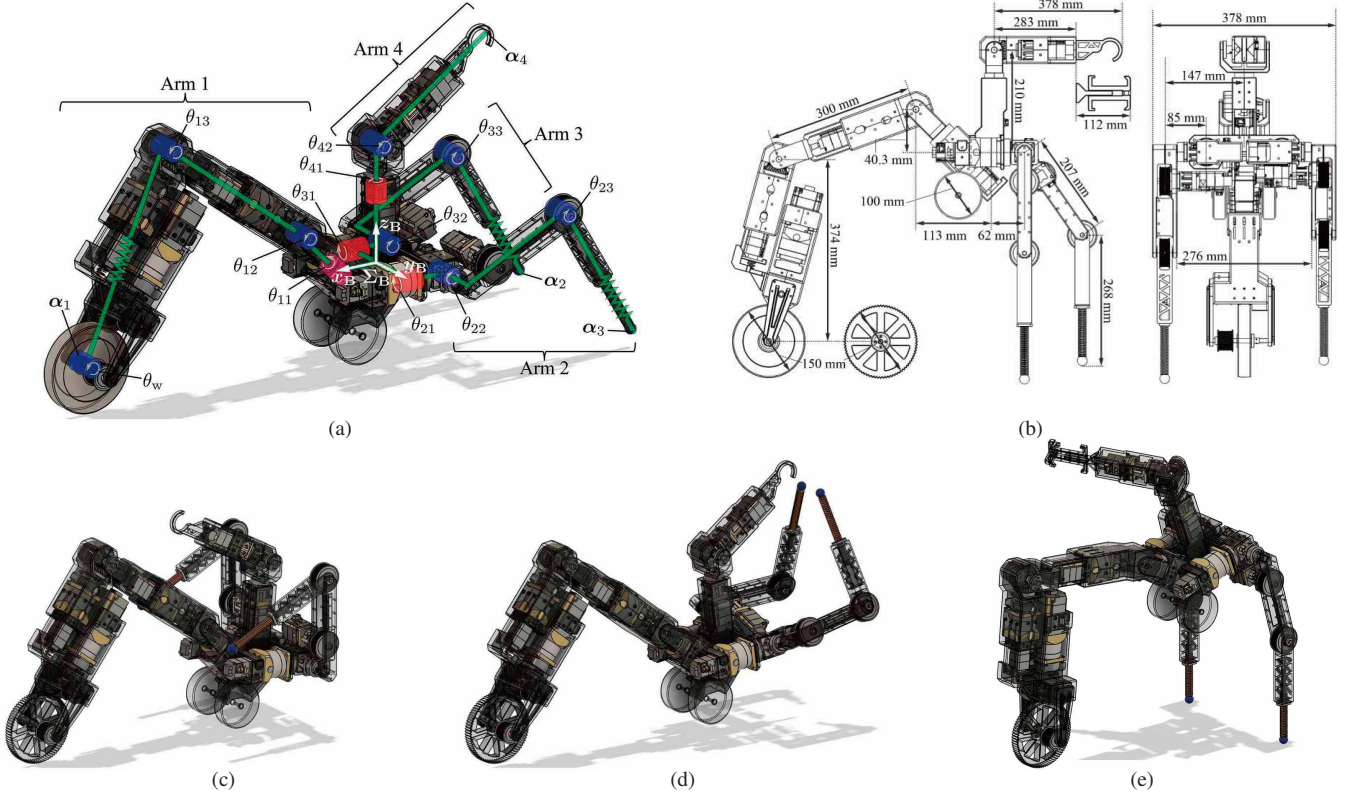


Fig. 2. Configuration of ARMS. (a) Joint configuration with wheel-legged walking mode. (b) Dimensions in the side and back views. (c) Wheel driving mode. (d) Wheel driving and grasping mode. (e) Standing mode.

mobility, and quad-arm manipulation with less DOF. Particularly, the tripedal legged mobility using a single active wheel and two legs is not unstable as bipedal mobility and not redundant as quadrupedal and hexapedal mobilities. Additionally, ARMS uses its arms for both mobility and manipulation similar to RoboSimian [11] and ALPHRED [12] and different from CENTAURO [13], ANYmal [14], [15], and BIT-NAZA II [16]. Furthermore, ARMS has a manipulation-dedicated upper arm unlike RoboSimian [11] and a single active wheel at the front arm and two passive wheels at the torso unlike ALPHRED [12], CENTAURO [13], ANYmal [14], [15], and BIT-NAZA II [16].

## II. MECHANICAL DESIGN

ARMS is composed of a torso, four arms, single active wheel, and two passive wheels. The configuration of ARMS is depicted in Fig. 2(a), which shows 11 joints: three joints  $\theta_{1j}$  for front Arm 1, three joints  $\theta_{2j}$  for rear Arm 2, three joints  $\theta_{3j}$  for rear Arm 3, and two joints  $\theta_{4j}$  for upper Arm 4; an active wheel  $\theta_w$  attached to the end-effector of Arm 1; and two passive wheels attached to the torso. The positions of the end-effectors of Arms 1, 2, 3, and 4 are  $\alpha_1$ ,  $\alpha_2$ ,  $\alpha_3$ , and  $\alpha_4$ , respectively, and the coordinate  $\Sigma_B$  is set to ARMS's torso. Arm 1 has a spring between the motors for  $\theta_{13}$  and  $\theta_w$ , and Arms 2 and 3 have a series elastic structure. Fig. 2(b) shows ARMS's dimensions in the side and back views on CAD images. As the two types of the active wheels and end-effectors shown in the images, they can be switched according

TABLE I  
JOINT SPECIFICATIONS.

		Minimum joint angle [deg]	Maximum joint angle [deg]	Maximum absolute speed [rad/s]	Maximum absolute torque [Nm]
Arm 1	$\theta_{11}$	-100	100	14.97	20.8
	$\theta_{12}$	-120	120	14.97	20.8
	$\theta_{13}$	-90	100	14.97	20.8
Arm 2	$\theta_{21}$	-90	30	14.97	20.8
	$\theta_{22}$	-110	110	14.97	10.6
	$\theta_{23}$	-120	120	14.97	10.6
Arm 3	$\theta_{31}$	-30	90	14.97	20.8
	$\theta_{32}$	-110	110	14.97	10.6
	$\theta_{33}$	-120	120	14.97	10.6
Arm 4	$\theta_{41}$	-180	180	14.97	10.6
	$\theta_{42}$	-115	115	14.97	10.6
Wheel	$\theta_w$	N/A	N/A	62.83	20.1

to terrain conditions and objective tasks. AC servo motors and amplifiers from Yaskawa Electric Corporation are employed as the actuators. The motors used for Arm 1 are SGM7A-01A6AHC01 for all joints; Arms 2 and 3 use SGM7A-01A6AHC01 for joints  $\theta_{21}$  and  $\theta_{31}$  and SGM7A-A5A6AHC01 for the others; Arm 4 consists of SGM7A-A5A6AHC01 for all joints; and the active wheel is driven by SGM7A-04A6AH101. Twelve amplifiers are selected from the three types: SGD7S-R70-F-00-A, SGD7S-R90-F-00-A, and SGD7S-2R8-F-00-A. The range and specification of the motors are summarized in TABLE I.

ARMS is designed on the basis of the concept of general-purpose arms for both hybrid mobility and manipu-

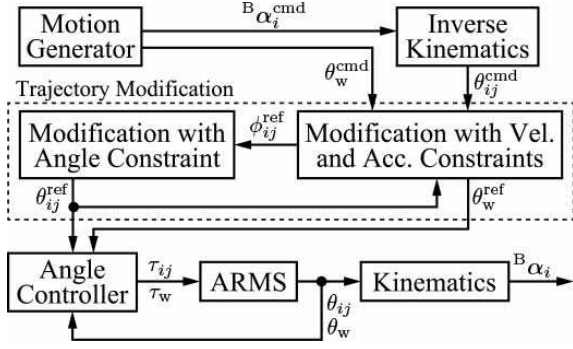


Fig. 3. Flow of the control system.

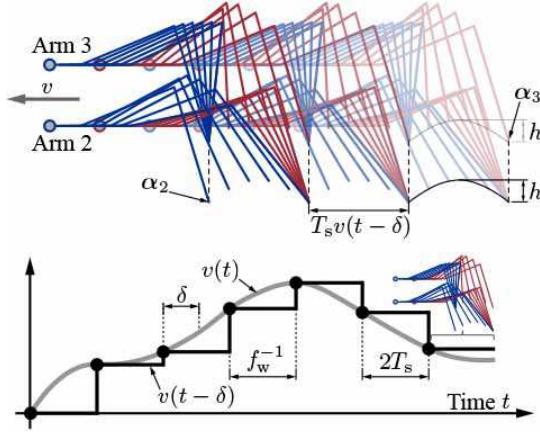


Fig. 4. Walking motion pattern.

lation capability. Accordingly, ARMS has four configurations: wheel-legged walking mode (Fig. 2(a)), wheel driving mode (Fig. 2(c)), wheel driving and grasping mode (Fig. 2(d)), and standing mode (Fig. 2(e)). In the configurations, Arm 1 is used for the wheeled mobility of the wheel-legged walking and wheel driving and for standing as a leg; Arms 2 and 3 are used for the legged walking, manipulation (grasping), and standing. Meanwhile, Arm 4 serves manipulation only. The wheel-legged walking mode is ARMS basic configuration, in which ARMS can move forward with the active wheel rotation and Arms 2 and 3's gait. For faster mobility on flat terrain, the wheel driving mode can move only with the active and passive wheels while ARMS can grasp and manipulate an object by coordinating Arms 2, 3, and 4 as the wheel driving and grasping mode. For performing tasks at an elevated position, ARMS can stand only with Arms 1, 2, and 3 and can manipulate Arm 4's end-effector. As the advantages of ARMS, all the walking, driving, and standing are realized by the three arms, which is more stable than a biped robot structure and results in less DOF than in quadrupedal robots.

### III. CONTROL DESIGN

ARMS is controlled as shown in Fig. 3, which includes a motion generator, inverse kinematics, a trajectory modification, and an angle controller. The motion generator provides the position command  ${}^B\alpha_i^{cmd}$  for each arm and the rotation

command  $\theta_w^{cmd}$  for the wheel. The inverse kinematics gives the angle commands  $\theta_{ij}^{cmd}$ , which satisfy the position commands  ${}^B\alpha_i^{cmd}$  for the arms. Through the trajectory modification, the commands  $\theta_{ij}^{cmd}$  and  $\theta_w^{cmd}$  are modified to the references  $\phi_{ij}^{ref}$  and  $\theta_w^{ref}$ , respectively, such that they are adapted for the velocity and acceleration constraints. Subsequently, the reference  $\phi_{ij}^{ref}$  is further modified to  $\theta_{ij}^{ref}$  that satisfies all the angle, velocity, and acceleration constraints. To track the reference values, the motor angles  $\theta_{ij}$  and  $\theta_w$  are controlled by proxy-based sliding mode control [27]–[29] in consideration of their torque saturation, and the angle controllers output the torque  $\tau_{ij}$  and  $\tau_w$  to the motors. For the simplification of the notations of the symbols, the subscript  $ij$  and  $w$  representing the joint is abbreviated below because the following computations are performed for each motor.

The motion generator provides the ARMS mobility and manipulation behaviors designed prior. For the wheel-legged tripedal walking, ARMS fixes Arm 1 configuration and swings Arms 2 and 3 alternatively according to the desired moving velocity  $v$  and walking frequency  $f_w$ , as illustrated in Fig. 4. The initial positions of Arms 2 and 3:  $\alpha_2$  and  $\alpha_3$  are the same; Arm 3 moves forward sinusoidally with the step length  $T_s v(t - \delta)$  and pre-determined height  $h$  while Arm 2 pushes ground; and Arm 2 follows Arm 3 subsequently. Fig. 4 illustrates the relationship of the variables also, and the step period  $T_s$  and delay  $\delta$  are determined as  $T_s = f_w^{-1}/2$  and  $\delta = t \bmod 2T_s$ , respectively. Additionally, for the wheel-legged tripedal walking and wheel driving, the angular velocity of the active wheel attached to the end-effector of Arm 1 is computed as  $\dot{\theta}_w^{ref} = 2v(t - \delta)/d$ , where  $d$  stands for the diameter of the active wheel.

The trajectory modification has two steps: modification with the velocity and acceleration constraints and modification with the angle constraint. In the first step, the command  $\theta_k^{cmd}$  is modified to the reference  $\phi_k^{ref}$  as

$$\phi_k^{ref} = \theta_{k-2}^{cmd} + e_k. \quad (1)$$

The modification term  $e_k$  is derived by quadratic programming that solves the following quadratic optimization problem with inequality constraints for the angular velocity and angular acceleration:

$$\begin{aligned} & \underset{e_k, e_{k+1}, e_{k+2}}{\text{minimize}} && e_k^2 + w_1 T^2 \dot{e}_{k+1}^2 + w_2 T^2 \dot{e}_{k+2}^2 \\ & \text{s.t.} && \phi_{k+h} = \theta_{k-2+h}^{cmd} + e_{k+h} \\ & && \phi_{k-1} = \theta_{k-1}^{ref}, \phi_{k-2} = \theta_{k-2}^{ref} \\ & && \dot{\phi}_{k+h} = (\phi_{k+h} - \phi_{k+h-1})/T \\ & && \ddot{\phi}_{k+h} = (\phi_{k+h} - 2\phi_{k+h-1} + \phi_{k+h-2})/T^2 \\ & && \dot{\theta}^{\min} \leq \dot{\phi}_{k+h} \leq \dot{\theta}^{\max}, \ddot{\theta}^{\min} \leq \ddot{\phi}_{k+h} \leq \ddot{\theta}^{\max} \\ & && h = 0, 1, 2. \end{aligned} \quad (2)$$

They are written in the discrete-time domain based on the backward difference with the sampling  $k$  and sampling time  $T$ , and the quadratic programming is solved at each sampling. The future modification terms  $e_{k+1}$  and  $e_{k+2}$  are considered to smooth the reference trajectory. In the second step, the obtained reference angle  $\phi_k^{ref}$  is further modified according



to the angle constraints without violating the velocity and acceleration constraints as

$$\theta_k^{\text{ref}} = \begin{cases} \phi_k^{\text{ref}} & \text{if } \theta_{\min} \leq \hat{\phi}_{k+L}^{\text{ref}} \leq \theta_{\max} \\ \theta_{k-1}^{\text{ref}} + T\dot{\theta}_{k-1}^{\text{ref}} + T^2\ddot{\theta}_k^{\text{ref}} & \text{otherwise} \end{cases} \quad (3a)$$

$$\ddot{\theta}_k^{\text{ref}} = \text{sat}_{(\ddot{\theta}_{\min}, \ddot{\theta}_{\max})}(-(\theta_{k-1}^{\text{ref}} - \theta_{k-2}^{\text{ref}})T^{-2}), \quad (3b)$$

where

$$L = \min\{l \in \mathbb{Z}_{\geq 0} | \dot{\phi}_k^{\text{ref}}(\dot{\phi}_k^{\text{ref}} + T\ddot{\theta}_k + (l-1)T\ddot{\theta}_k) \leq 0\}$$

$$\hat{\phi}_k^{\text{ref}} = \phi_k^{\text{ref}}, \quad \hat{\phi}_{k+1}^{\text{ref}} = C(A\Phi_k^{\text{ref}} + B\ddot{\theta}_k)$$

$$\hat{\phi}_{k+L|L>1}^{\text{ref}} = CA^L\Phi_k^{\text{ref}} + CA^{L-1}B\ddot{\theta}_k + C \sum_{i=0}^{L-2} A^i B\ddot{\theta}_k$$

$$\Phi_k^{\text{ref}} = \begin{bmatrix} \phi_k^{\text{ref}} \\ \dot{\phi}_k^{\text{ref}} \end{bmatrix}, \quad A = \begin{bmatrix} 1 & T \\ 0 & 1 \end{bmatrix}, \quad B = \begin{bmatrix} 0 \\ T \end{bmatrix}$$

$$C = \begin{bmatrix} 1 & 0 \end{bmatrix}, \quad \text{sat}_{(a, b)}(x) = \begin{cases} a & \text{if } x < a \\ x & \text{if } a \leq x \leq b \\ b & \text{if } x > b \end{cases}$$

$$\ddot{\theta}_k = \begin{cases} \ddot{\theta}_{\max} & \text{if } \dot{\phi}_k^{\text{ref}} > 0 \\ 0 & \text{if } \dot{\phi}_k^{\text{ref}} = 0 \\ \ddot{\theta}_{\min} & \text{if } \dot{\phi}_k^{\text{ref}} < 0 \end{cases}, \quad \ddot{\theta}_k = \begin{cases} \ddot{\theta}_{\min} & \text{if } \dot{\phi}_k^{\text{ref}} > 0 \\ 0 & \text{if } \dot{\phi}_k^{\text{ref}} = 0 \\ \ddot{\theta}_{\max} & \text{if } \dot{\phi}_k^{\text{ref}} < 0 \end{cases}$$

Here,  $L$  denotes the deceleration time until sign reversal of the reference velocity  $\dot{\phi}_k^{\text{ref}}$ , which is composed of initial maximum acceleration  $\ddot{\theta}_k$  at  $k+1$  and subsequent maximum deceleration  $\ddot{\theta}_k$  from  $k+2$  to  $k+L$ . If the angle violates the angle constraints  $\theta_{\min} \leq \hat{\phi}_{k+L}^{\text{ref}} \leq \theta_{\max}$  after the deceleration, the acceleration  $\ddot{\theta}_k^{\text{ref}}$  is set to bring the velocity  $\dot{\theta}_k^{\text{ref}}$  to zero with acceleration saturation as (3b), which attains  $\dot{\theta}_k^{\text{ref}} = \dot{\theta}_{k-1}^{\text{ref}} + T\ddot{\theta}_k^{\text{ref}} = 0$  while unsaturated and decelerates to zero while saturated.

The angle controller uses the proxy-based sliding mode control [27]–[29], which seamlessly changes proportional-integral-derivative angle control with fast reference tracking, force saturation in the reaching mode, and smooth convergence to the reference angle after the saturation in the sliding mode. The continuous-time representation of the controller is

$$\tau = M\ddot{p} - B\ddot{\alpha} - K\dot{\alpha} - L\alpha \quad (4a)$$

$$\tau \in \text{sgn}_F(-J\ddot{\beta} - H\dot{\beta} - \beta) \quad (4b)$$

$$\dot{\alpha} = \theta - p, \quad \beta = p - \theta^{\text{ref}}, \quad (4c)$$

where  $M$  and  $F$  are the moment of inertia and force limit of the motors, respectively. The proportional-integral-derivative controller (4a) is dominant during unsaturation, and the sliding mode controller (4b) based on the set-valued sign function

$$\text{sgn}_F(x) = \begin{cases} \{-F\} & \text{if } x < 0 \\ [-F, F] & \text{if } x = 0 \\ \{F\} & \text{if } x > 0 \end{cases}$$

is dominant during saturation and after the saturation. By using the proxy-based sliding mode control, we can design an unsaturated response with the proportional-integral-derivative gains  $B$ ,  $K$ , and  $L$ , can implement saturation as a part of the sliding mode controller, and can design the response after the saturation with the gains  $J$  and  $H$  of the switching function  $-J\ddot{\beta} - H\dot{\beta} - \beta$ .

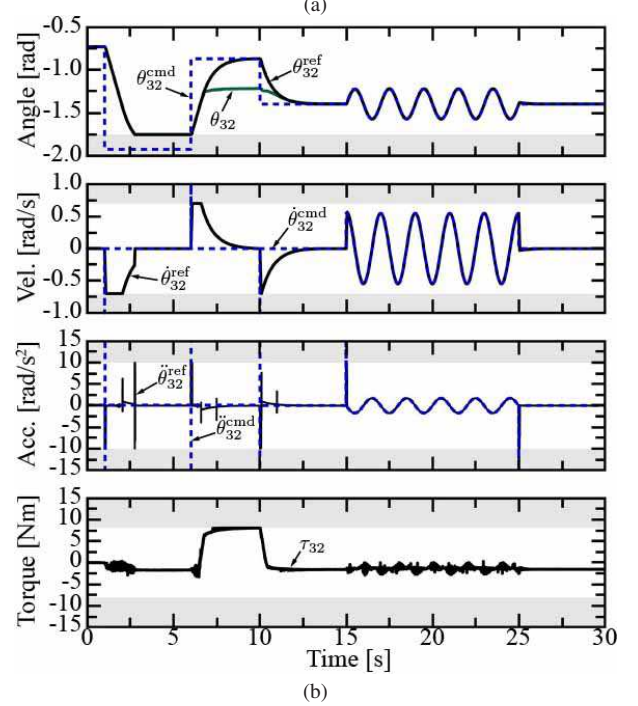


Fig. 5. Validation of the trajectory modification (1)–(3) and proxy-based sliding mode controller (4). (a) Contact motion in 6–10 s. (b) Results of the joint  $\theta_{32}$ .

The trajectory modification and the angle controller were experimentally validated with Arm 3, as shown in Fig. 5. In this validation, the minimum joint constraint was set to -1.75 rad, and the torque saturation was set to 60 % of the maximum and minimum values. The command  $\theta_{32}^{\text{cmd}}$  was not smooth and yielded the impulsive velocity  $\dot{\theta}_{32}^{\text{cmd}}$  and acceleration  $\ddot{\theta}_{32}^{\text{cmd}}$ , which violated the angle, velocity, and acceleration constraints. The command angle  $\theta_{32}^{\text{cmd}}$  was modified by the trajectory modification to the reference angle  $\theta_{32}^{\text{ref}}$ , and the angle response  $\theta_{32}$  tracked the reference angle with the angle controller (4). The reference angle  $\theta_{32}^{\text{ref}}$  was adjusted to satisfy the angle constraints in 1–6 s, and the reference angular velocity and acceleration:  $\dot{\theta}_{32}^{\text{ref}}$  and  $\ddot{\theta}_{32}^{\text{ref}}$  also satisfied their constraints at 1, 6, and 10 s, as shown in Fig. 5(b). In 6–10 s, the arm contacted with the ground as Fig. 5(a) and did not reach the reference angle owing to the saturated torque  $\tau_{32}$ . The angle response  $\theta_{32}$  gradually returned to the reference angle  $\theta_{32}^{\text{ref}}$  after the saturation in the sliding mode. In 15–25 s, the angle response tracked the sin command precisely with the controller while the command did not violate the constraints.

#### IV. EXPERIMENTS

We conducted four experiments that validated the hybrid mobility and task capability of ARMS with the legged mobil-

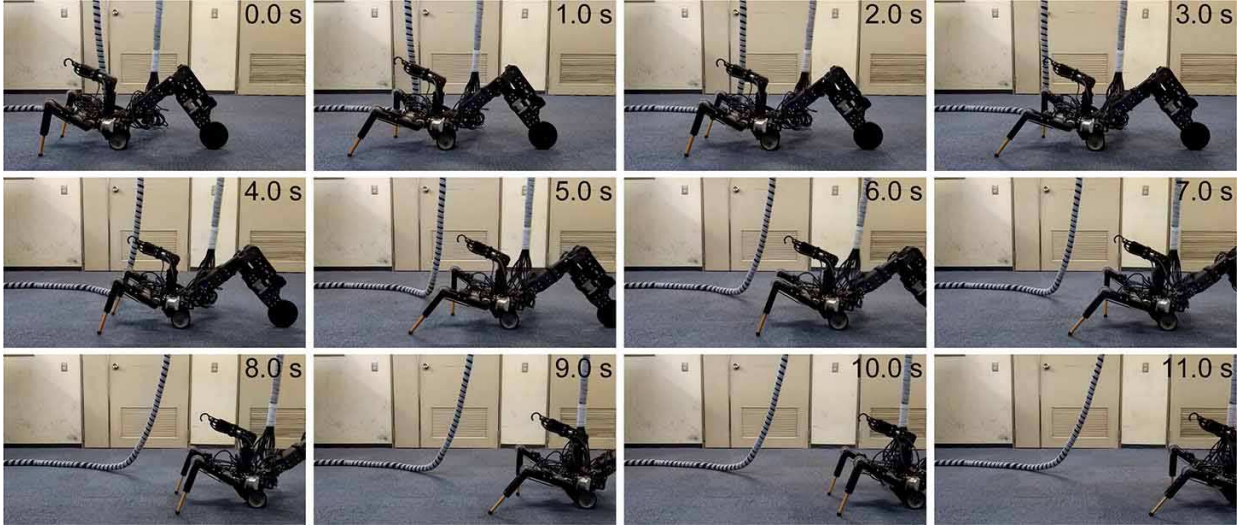


Fig. 6. Result of wheel-legged walking.

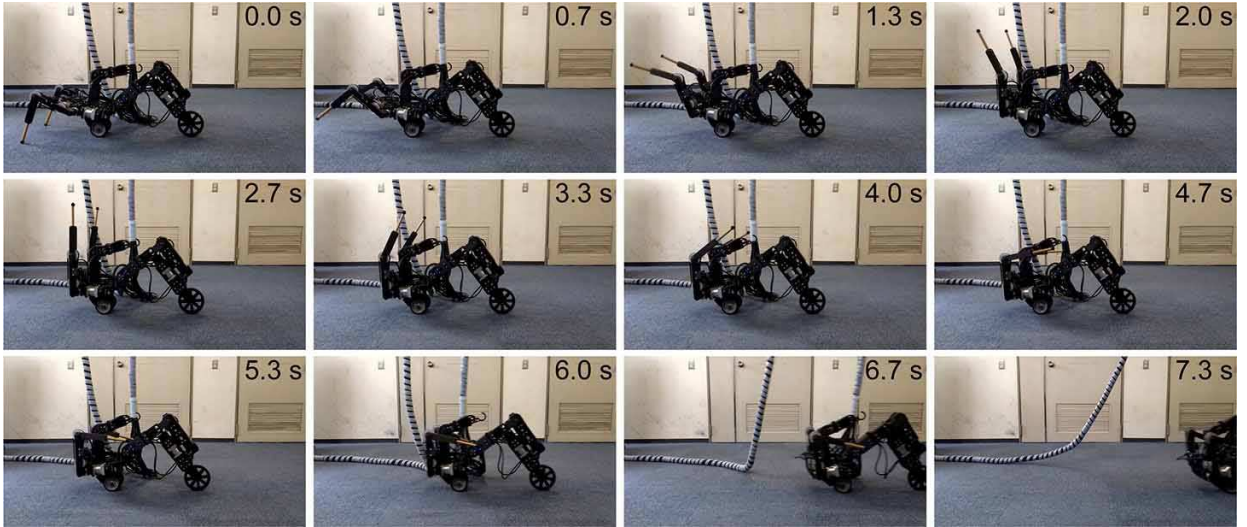


Fig. 7. Result of wheel driving.

ity, wheeled mobility, and manipulation coordinating the four arms.

- Task 1) Wheel-legged walking
- Task 2) Wheel driving
- Task 3) Wheel driving with grasping
- Task 4) Carrying a bag

In the experiments, the controller shown in Fig. 3 was implemented on a PC with Linux OS and RTAI, which had two real-time threads: the thread for the angle controller with the sampling time 0.25 ms and that for the other computations with the sampling time 0.5 ms.

Fig. 6 shows the result of the wheel-legged walking task. In this task, ARMS walked using the active wheel attached to Arm 1, passive wheels attached to the torso, and Arms 2 and 3. ARMS began walking at 0 s; the active wheel rotated and Arms 2 and 3 swung alternately according to the desired moving velocity in 0–11 s. Although the experiment

was conducted on a flat terrain, the legged mobility using Arms 2 and 3 is expected to be effective on a non-flat terrain as well.

Fig. 7 shows the result of the wheel driving task. ARMS started to transform its configuration from the walking configuration to the driving configuration at 0 s, and Arms 2 and 3 moved accordingly from 0 to 5 s. Subsequently, ARMS moved forward using its active and passive wheels attached to Arm 1 and the torso, respectively. This result validated that ARMS has the faster mobility with the wheels on a flat terrain than the legged mobility as Fig. 6.

Fig. 8 shows the result of the task of wheel driving with grasping. Arms 2, 3, and 4 grasped a yellow bowl given by an experimenter from 0 to 10 s. Then, ARMS moved forward while grasping the bowl from 10 to 19 s.

Fig. 9 shows the result of the task of carrying a bag. ARMS raised the torso with the three arms from 0 to 8 s, picked up



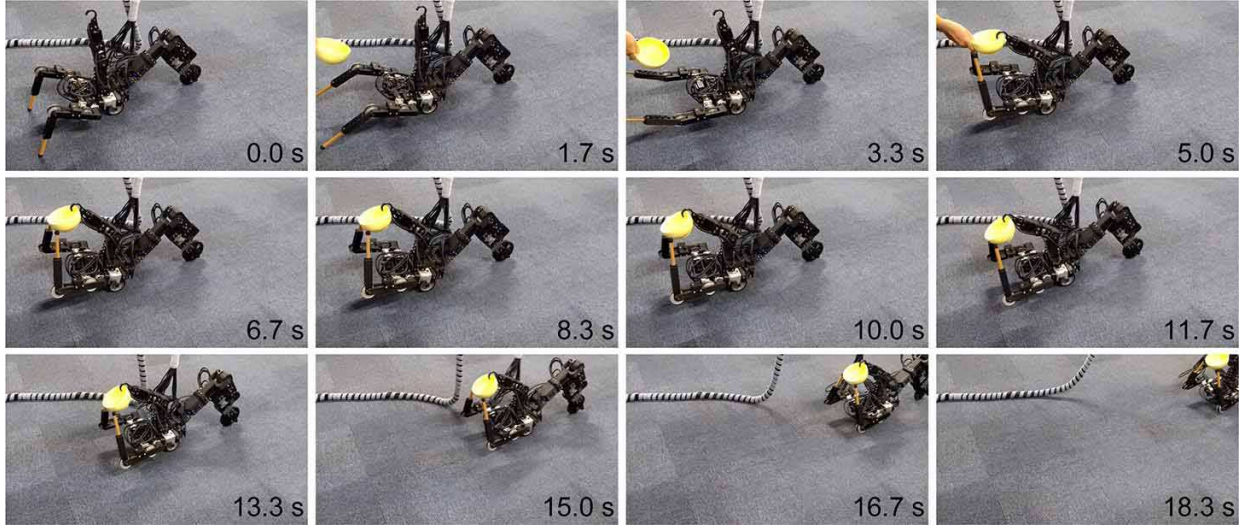


Fig. 8. Result of wheel driving with grasping.

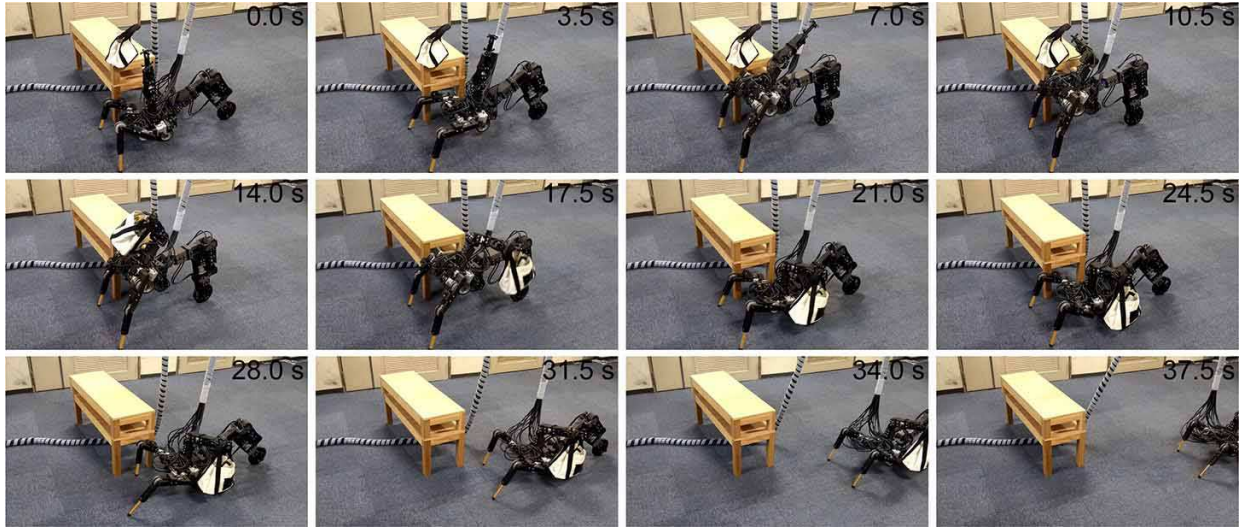


Fig. 9. Result of carrying a bag.

the bag by using Arm 4 from 8 to 18 s, and lowered the torso from 18 to 22 s while holding the bag. Subsequently, ARMS carried the bag forward by wheel-legged walking.

The developed robot has two limitations. First, although ARMS requires servo amplifiers and a PC, the electrical system and the PC are not mounted on the robot. This leads to a limited movable range of ARMS due to the motor cables, which are suspended from above, as shown in the figures for the results. Second, a device for sending operator commands to ARMS controller in real time is not implemented. Consequently, it is necessary to design the motion generator shown in Fig. 3 prior to the experiments.

## V. CONCLUSION

This letter proposed the mobile quad-arm robot: ARMS and showed the mechanical and control design for ARMS. The unified wheel-legged tripodal mobility, wheeled mobility, and

quad-arm manipulation of ARMS were experimentally validated through the following four tasks: wheel-legged walking, wheel-driving, wheel-driving with grasping, and carrying a bag.

## REFERENCES

- [1] N. Kau, A. Schultz, N. Ferrante, and P. Slade, "Stanford Doggo: An open-source, quasi-direct-drive quadruped," in *Proc. IEEE Int. Conf. Robot. Autom.*, May 2019, pp. 6309–6315.
- [2] J. Kim, T. Kang, D. Song, and S.-J. Yi, "Design and control of a open-source, low cost, 3D printed dynamic quadruped robot," *Appl. Sci.*, vol. 11, no. 9, Apr. 2021.
- [3] Y. H. Lee, Y. H. Lee, H. Lee, H. Kang, J. H. Lee, L. T. Phan, S. Jin, Y. B. Kim, D.-Y. Seok, S. Y. Lee, H. Moon, J. C. Koo, and H. R. Choi, "Development of a quadruped robot system with torque-controllable modular actuator unit," *IEEE Trans. Ind. Electron.*, vol. 68, no. 8, pp. 7263–7273, Aug. 2021.
- [4] P. Arm, R. Zenkl, P. Barton, L. Beglinger, A. Dietsche, L. Ferrazzini, E. Hampp, J. Hinder, C. Huber, D. Schaufelberger, F. Schmitt, B. Sun, B. Stolz, H. Kolvenbach, and M. Hutter, "SpaceBok: A dynamic legged

- robot for space exploration,” in *Proc. IEEE Int. Conf. Robot. Autom.*, May 2019, pp. 6288–6294.
- [5] P. Čížek, M. Zoula, and J. Faigl, “Design, construction, and rough-terrain locomotion control of novel hexapod walking robot with four degrees of freedom per leg,” *IEEE Access*, vol. 9, pp. 17 866–17 881, Jan. 2021.
  - [6] T. Takaki, T. Aoyama, and I. Ishii, “Development of inverted pendulum robot capable of climbing stairs using planetary wheel mechanism,” in *Proc. IEEE Int. Conf. Robot. Autom.*, May 2013, pp. 5618–5624.
  - [7] X. Zhang, Y. Xie, L. Jiang, G. Li, J. Meng, and Y. Huang, “Fault-tolerant dynamic control of a four-wheel redundantly-actuated mobile robot,” *IEEE Access*, vol. 7, pp. 157 909–157 921, Nov. 2019.
  - [8] K. Kaneko, H. Kaminaga, T. Sakaguchi, S. Kajita, M. Morisawa, I. Kumagai, and F. Kanehiro, “Humanoid robot HRP-5P: An electrically actuated humanoid robot with high-power and wide-range joints,” *IEEE Robot. Autom. Lett.*, vol. 4, no. 2, pp. 1431–1438, Jan. 2019.
  - [9] J. Engelsberger, A. Werner, C. Ott, B. Henze, M. A. Roa, G. Garofalo, R. Burger, A. Beyer, O. Eiberger, K. Schmid, and A. Albu-Schäffer, “Overview of the torque-controlled humanoid robot TORO,” in *Proc. IEEE-RAS Int. Conf. Humanoid Robots*, Feb. 2014, pp. 916–923.
  - [10] O. Stasse, T. Flayols, R. Budhiraja, K. Giraud-Esclasse, J. Carpentier, J. Mirabel, A. Del Prete, P. Souères, N. Mansard, F. Lamiriaux, J.-P. Laumond, L. Marchionni, H. Tome, and F. Ferro, “TALOS: A new humanoid research platform targeted for industrial applications,” in *Proc. IEEE-RAS Int. Conf. Humanoid Robots*, Jan. 2017, pp. 689–695.
  - [11] P. Hebert, M. Bajracharya, J. Ma, N. Hudson, A. Aydemir, J. Reid, C. Bergh, J. Borders, M. Frost, M. Hagman, J. Leichty, P. Backes, B. Kennedy, P. Karplus, B. Satzinger, K. Byl, K. Shankar, and J. Burdick, “Mobile manipulation and mobility as manipulation—design and algorithms of RoboSimian,” *J. Field Robot.*, vol. 32, no. 2, pp. 255–274, Feb. 2015.
  - [12] J. Hooks, M. S. Ahn, J. Yu, X. Zhang, T. Zhu, H. Chae, and D. Hong, “ALPHRED: A multi-modal operations quadruped robot for package delivery applications,” *IEEE Robot. Autom. Lett.*, vol. 5, no. 4, pp. 5409–5416, Jun. 2020.
  - [13] N. Kashiri, L. Baccelliere, L. Muratore, A. Laurenzi, Z. Ren, E. M. Hoffman, M. Kamedula, G. F. Rigano, J. Malzahn, S. Cordasco, P. Guria, A. Margan, and N. G. Tsarakis, “CENTAURO: A hybrid locomotion and high power resilient manipulation platform,” *IEEE Robot. Autom. Lett.*, vol. 4, no. 2, pp. 1595–1602, Apr. 2019.
  - [14] M. Bjelonic, C. D. Bellicoso, Y. de Viragh, D. Sako, F. D. Tresoldi, F. Jenelten, and M. Hutter, “Keep rollin’—whole-body motion control and planning for wheeled quadrupedal robots,” *IEEE Robot. Autom. Lett.*, vol. 4, no. 2, pp. 2116–2123, Apr. 2019.
  - [15] V. S. Medeiros, E. Jelavic, M. Bjelonic, R. Siegwart, M. A. Meggiolaro, and M. Hutter, “Trajectory optimization for wheeled-legged quadrupedal robots driving in challenging terrain,” *IEEE Robot. Autom. Lett.*, vol. 5, no. 3, pp. 4172–4179, Apr. 2020.
  - [16] Z. Chen, S. Wang, J. Wang, K. Xu, T. Lei, H. Zhang, X. Wang, D. Liu, and J. Si, “Control strategy of stable walking for a hexapod wheel-legged robot,” *ISA Trans.*, vol. 108, pp. 367–380, Aug. 2021.
  - [17] K. Nagano and Y. Fujimoto, “Simplification of motion generation in the singular configuration of a wheel-legged mobile robot,” *IEEE J. Ind. Appl.*, vol. 8, no. 5, pp. 745–755, Sep. 2019.
  - [18] C. Zhang, T. Liu, S. Song, J. Wang, and M. Q.-H. Meng, “Dynamic wheeled motion control of wheel-biped transformable robots,” *Biomimetic Intell. Robot.*, vol. 2, no. 2, p. 100027, Nov. 2022.
  - [19] C. Zhang, T. Liu, S. Song, and M. Q.-H. Meng, “System design and balance control of a bipedal leg-wheeled robot,” in *Proc. IEEE-RAS Int. Conf. Robot. Biomimetics*, Dec. 2019, pp. 1869–1874.
  - [20] V. Klemm, A. Morra, C. Salzmann, F. Tschopp, K. Bodie, L. Gulich, N. Küng, D. Mannhart, C. Pfister, M. Vierneisel, F. Weber, R. Deuber, and R. Siegwart, “Ascento: A two-wheeled jumping robot,” in *Proc. IEEE Int. Conf. Robot. Autom.*, May 2019, pp. 7515–7521.
  - [21] X. Qiu, Z. Yu, L. Meng, X. Chen, L. Zhao, G. Huang, and F. Meng, “Upright and crawling locomotion and its transition for a wheel-legged robot,” *Micromachines*, vol. 13, no. 8, Aug. 2022.
  - [22] E. C. Orozco-Magdaleno, F. Gómez-Bravo, E. Castillo-Castañeda, and G. Carbone, “Evaluation of locomotion performances for a mecatronics-wheeled hybrid hexapod robot,” *IEEE/ASME Trans. Mechatronics*, vol. 26, no. 3, pp. 1657–1667, Sep. 2021.
  - [23] K. Tadakuma, R. Tadakuma, A. Maruyama, E. Rohmer, K. Nagatani, K. Yoshida, A. Ming, M. Shimojo, M. Higashimori, and M. Kaneko, “Mechanical design of the wheel-leg hybrid mobile robot to realize a large wheel diameter,” in *Proc. IEEE Int. Conf. on Intelligent Robots and Systems*, Oct. 2010, pp. 3358–3365.
  - [24] W.-H. Chen, H.-S. Lin, Y.-M. Lin, and P.-C. Lin, “TurboQuad: A novel leg-wheel transformable robot with smooth and fast behavioral transitions,” *IEEE Trans. Robot.*, vol. 33, no. 5, pp. 1025–1040, May 2017.
  - [25] C. Zheng and K. Lee, “WheelLeR: Wheel-leg reconfigurable mechanism with passive gears for mobile robot applications,” in *Proc. IEEE Int. Conf. Robot. Autom.*, May 2019, pp. 9292–9298.
  - [26] Y. Kim, Y. Lee, S. Lee, J. Kim, H. S. Kim, and T. Seo, “STEP: A new mobile platform with 2-DOF transformable wheels for service robots,” *IEEE/ASME Trans. Mechatronics*, vol. 25, no. 4, pp. 1859–1868, Aug. 2020.
  - [27] R. Kikuuwe and H. Fujimoto, “Proxy-based sliding mode control for accurate and safe position control,” in *Proc. IEEE Int. Conf. Robot. Autom.*, May 2006, pp. 25–30.
  - [28] R. Kikuuwe, S. Yasukouchi, H. Fujimoto, and M. Yamamoto, “Proxy-based sliding mode control: A safer extension of PID position control,” *IEEE Trans. Robot.*, vol. 26, no. 4, pp. 670–683, Aug. 2010.
  - [29] R. Kikuuwe, “A sliding-mode-like position controller for admittance control with bounded actuator force,” *IEEE/ASME Trans. Mechatronics*, vol. 19, no. 5, pp. 1489–1500, Oct. 2014.